CrossMark

Classifying Optical (Out)bursts in Cataclysmic Variables: The Distinct Observational Characteristics of Dwarf Novae, Micronovae, Stellar Flares, and Magnetic Gating

Krystian Iłkiewicz[1,2] , Simone Scaringi[2] , Martina Veresvarska[2] , Domitilla De Martino[3] , Colin Littlefield[4] ,
Christian Knigge[5] , John A. Paice[2] , and Anwesha Sahu[6]

[1] Astronomical Observatory, University of Warsaw, Al. Ujazdowskie 4, 00-478 Warszawa, Poland
[2] Centre for Extragalactic Astronomy, Department of Physics, Durham University, DH1 3LE, UK
[3] INAF-Osservatorio Astronomico di Capodimonte, salita Moiariello 16, I-80131, Napoli, Italy
[4] Department of Physics, University of Notre Dame, Notre Dame, IN 46556, USA
[5] Department of Physics and Astronomy. University of Southampton, Southampton SO17 1BJ, UK
[6] Department of Physics, University of Warwick, Gibbet Hill Road, Coventry CV4 7AL, UK

Abstract

Cataclysmic variables can experience short optical brightenings, which are commonly attributed to phenomena such as dwarf novae outbursts, micronovae, donor flares, or magnetic gating bursts. Since these events exhibit similar observational characteristics, their identification has often been ambiguous. In particular, magnetic gating bursts and micronovae have been suggested as alternative interpretations of the same phenomena. Here we show that the timescales and energies separate the optical brightenings into separate clusters consistent with their different classifications. This suggests that micronovae and magnetic gating bursts are in fact separate phenomena. Based on our findings, we develop diagnostic diagrams that can distinguish between these bursts/flares based on their properties. We demonstrate the effectiveness of this approach on observations of a newly identified intermediate polar, CTCV J0333-4451, which we classify as a magnetic gating system. CTCV J0333-4451 is the third highest spin-to-orbital period ratio intermediate polar with magnetic gating, suggesting that these bursts are common among these rare systems.

1. Introduction

Cataclysmic variables (CVs) are binary stars in which an accreting white dwarf accretes material typically from a main-sequence mass donor. CVs can exhibit various forms of short optical bursts. Among the best-studied bursts in CVs are dwarf novae. Dwarf nova eruptions are caused by a thermal-viscous instability in the accretion disk (Lasota 2001). Based on the properties of the bursts, dwarf novae are divided into several subtypes (e.g., Warner 2003). However, their duration and amplitude depend mainly on the size of the accretion disk. In particular, their duration can range from a few days (e.g., Cannizzo et al. 2012) to years (e.g., Iłkiewicz et al. 2023).

In CVs with a magnetic white dwarf, the accretion disk is truncated. This makes dwarf novae outbursts less likely to occur in magnetic systems compared to nonmagnetic CVs (Hameury & Lasota 2017). In these magnetic systems, two other kinds of bursts seem more likely: micronovae and magnetic gating bursts. Micronovae occur on timescales of hours, show energies 10^{-6} times smaller compared to classical novae, and have outburst shapes similar to Type I X-ray bursts in accreting neutron stars (Scaringi et al. 2022b). The proposed mechanism behind micronovae is localized thermonuclear runaways in magnetically confined accretion streams (Scaringi et al. 2022a). Another explanation for micronovae could be magnetic reconnection events in the magnetic disk (Schaefer et al. 2022). On the other hand, in the magnetic gating model,

accretion is halted by the white dwarf magnetic field until enough pressure builds up in the accretion disk allowing for a short burst of accretion (D'Angelo & Spruit 2010, 2012; Scaringi et al. 2017). While magnetic gating is a widely accepted phenomenon, the reality of micronovae is still under question. In particular, magnetic gating bursts have been proposed as an alternative interpretation of the claimed micronovae (Hameury et al. 2022).

Among the most rare short brightenings observed in CVs are stellar flares originating from the mass donor (Ramsay et al. 2021). They are expected to have similar properties to flares and superflares from single stars. However, they are rarely observed in CVs. This is likely because the mass donor is tidally locked, making it spin rapidly, and rapidly rotating main-sequence stars are unlikely to show flaring activity (Ramsay et al. 2020).

Here we explore the observational properties of short optical bursts in CVs. Based on the studied systems we discover that the short bursts observed in CVs fall into separate clusters based on their burst energies and timescales. In particular, we show that magnetic gating systems and micronovae display distinct sets of characteristics, implying different physical mechanisms are at play in these bursts. Based on our findings, we advocate the use of diagnostic diagrams to identify the nature of a given burst. We employ the newly proposed method to classify bursts in the newly identified intermediate polar CTCV J0333-4451 (hereafter J0333). We show that J0333 falls in the cluster of magnetic gating systems.
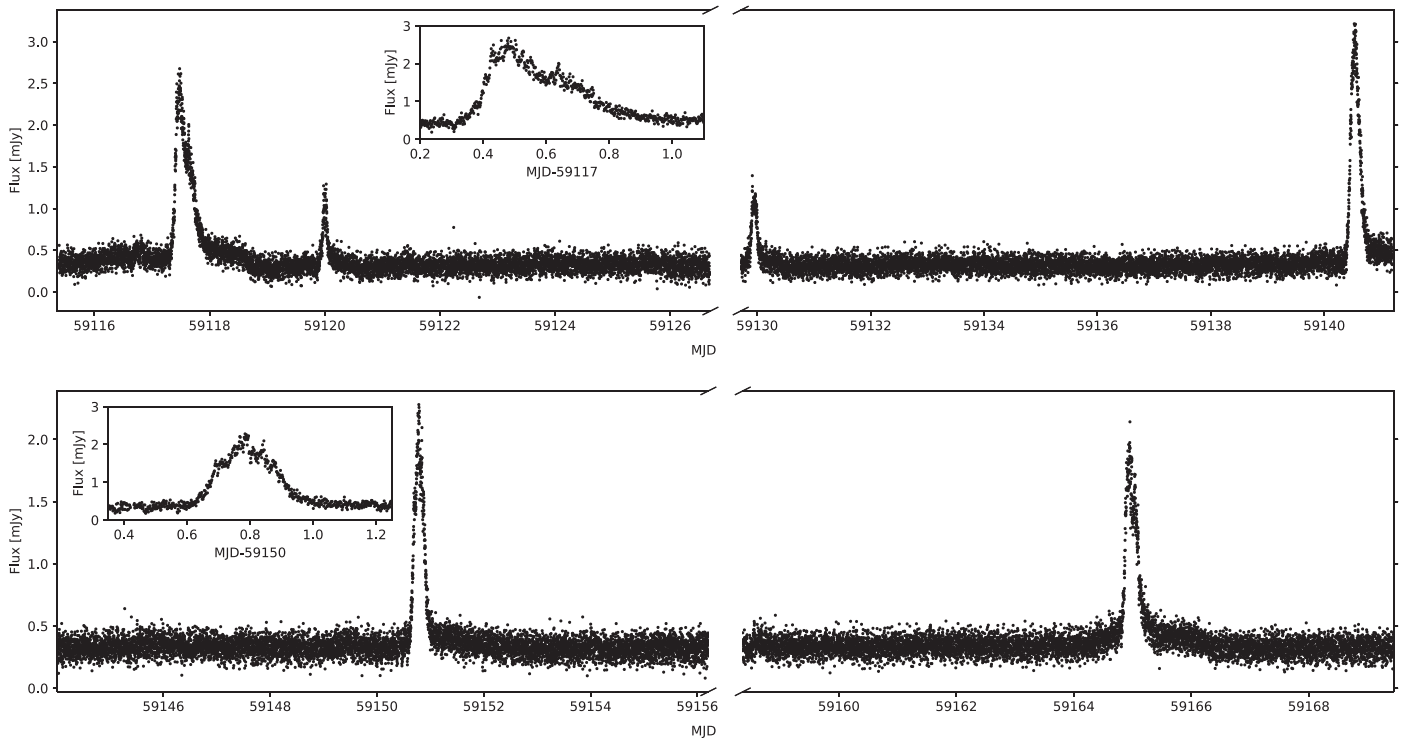
Figure 1. Sectors 30 (top) and 31 (bottom) of the TESS observations of J0333 with flux scale calibrated to the ASAS-SN g filter. The top inset figure shows a zoom on an asymmetrical burst, while the bottom inset figure shows a symmetrical burst.

2. Observations and Literature Data

We employed observations of J0333 made by the Transiting Exoplanet Survey Satellite (TESS; Ricker et al. 2015). The observations were carried out during TESS sectors 30 and 31 (2020 September 23–November 18) with a 120 s cadence. The data were processed with the Science Processing Operations Center pipeline (Jenkins et al. 2016).

In order to flux-calibrate TESS observations we followed a method employed by Scaringi et al. (2022b). Namely, we found nearly simultaneous observations of TESS and ASAS-SN. Then, we fitted a linear relationship between the TESS simple aperture photometry flux in electrons per second and ASAS-SN flux in the g band. We then used this relationship to scale the TESS data to fluxes in Jy. The J0333 light curve is presented in Figure 1. We employed the same flux-calibration method with TESS data of J0333 and observations of other objects.

Here we consider properties of short bursts observed in CVs, i.e., bursts with duration of order of days or shorter. Due to the short timescales of the bursts, we limited the comparison to bursts observed with Kepler and TESS, where the cadence is higher and more consistent compared to ground-based observations. Our analysis is intended for CVs with short orbital periods ($<$10 hr) and will have limited application to CVs with evolved donors. This is because evolved stars can experience stellar flares that have energies similar to the energies of micronovae (see, e.g., Figure 9 of Tu et al. 2021). However, the only CV with short bursts and a long orbital period observed by either TESS or Kepler is V2487 Oph, with the distance to the object being too uncertain for a meaningful analysis (Schaefer et al. 2022). In order to estimate the energies of bursts in each system we assumed distances based on a Gaia Data Release 3 (DR3) parallax (Bailer-Jones et al. 2021). We

also exclude classical novae from our analysis, even though they can occur on short timescales (e.g., Sokolovsky et al. 2023). This is because classical novae have luminosities several orders of magnitude larger compared to other bursts in CVs. We assume that interstellar reddening to all of the systems is negligible. This is consistent with extinction $A_g < 0.4$ mag estimated with a 3D reddening map for all objects for which data were available (Green et al. 2019).

In order to measure the properties of short bursts in CVs, we reanalyzed already-published TESS observations of V1025 Cen (Littlefield et al. 2022) and TW Pic (Scaringi et al. 2022c). Moreover, in order to measure individual bursts in MV Lyr, we flux calibrated the Kepler light curve to the V band using the calibration of Scaringi et al. (2017). In the case of TV Col, EI UMa, and ASASSN-19bh, we corrected the published burst peak luminosities by subtracting the quiescent flux of the systems (Scaringi et al. 2022b). The measurements of burst in CP Pup are directly taken from Veresvarska et al. (2024). We supplemented our sample with dwarf novae outbursts reported by Otulakowska-Hypka et al. (2016) that had a duration of 7 days or less and were observed by TESS. We note that the constraints on the duration of outbursts exclude most intermediate polars with suspected dwarf-nova-type outbursts (e.g., GK Per, V455 And). However, we measured a suspected dwarf nova outburst in one intermediate polar, FS Aur.

We compared the bursts in CVs to stellar flares from main-sequence stars as they can occur on similar timescales. The only CV with flares originating from the donor observed by TESS is MQ Dra (Ramsay et al. 2021). MQ Dra was below the detection limit of ASAS-SN during the TESS observations. Hence, we employed the Zwicky Transient Facility (Masci et al. 2019) observations in the g filter to flux calibrate TESS data. Since main-sequence stars can experience superflares that

Table 1
Properties of Short Optical Bursts Observed in CVs Together with the Reference to the Source of Their Identification

Object	Outburst Type	Peak Optical Luminosity (erg s^{-1})	Total Optical Energy (erg)	Burst Duration (days)	Frequency (day^{-1})	Reference
J0333	Magnetic gating	$(0.9 \pm 0.5) \times 10^{32}$	$(13.2 \pm 9.8) \times 10^{35}$	0.58 ± 0.18	0.13	(1)
TW Pic	Magnetic gating	$(1.5 \pm 0.3) \times 10^{32}$	$(1.9 \pm 1.2) \times 10^{35}$	0.05 ± 0.03	16.11	(2)
MV Lyr	Magnetic gating	$(3.0 \pm 0.7) \times 10^{32}$	$(8.7 \pm 4.3) \times 10^{35}$	0.12 ± 0.03	6.39	(3)
V1025 Cen	Magnetic gating	$(0.9 \pm 0.1) \times 10^{32}$	$(4.6 \pm 3.5) \times 10^{35}$	0.36 ± 0.06	0.35	(4)
TV Col	Micronova	$(0.8 \pm 0.2) \times 10^{34}$	$(1.2 \pm 0.5) \times 10^{38}$	0.52 ± 0.13	0.05	(5)
EI UMa	Micronova	$(1.9 \pm 0.2) \times 10^{34}$	$(2.6 \pm 0.3) \times 10^{38}$	0.36 ± 0.07	0.04	(5)
ASASSN-19bh	Micronova	3.4×10^{34}	11.6×10^{38}	6.96	0.04	(5)
CP Pup	Micronova	$(0.32 \pm 0.06) \times 10^{34}$	0.6×10^{38}	0.8 ± 0.2	0.017	(6)
MQ Dra	Donor flare	2.6×10^{30}	2.2×10^{33}	0.035	0.012	(7)
V1504 Cyg	Dwarf nova	$(3.6 \pm 1.3) \times 10^{32}$	$(4.4 \pm 0.3) \times 10^{37}$	4.3 ± 0.2	0.09	(8)
IX Dra	Dwarf nova	$(2.2 \pm 0.4) \times 10^{32}$	$(2.5 \pm 0.6) \times 10^{37}$	3.9 ± 0.2	0.14	(8)
WX Hyi	Dwarf nova	$(1.5 \pm 0.2) \times 10^{32}$	$(1.3 \pm 0.3) \times 10^{37}$	2.8 ± 0.4	0.18	(8)
SS UMi	Dwarf nova	$(8.8 \pm 0.3) \times 10^{31}$	$(8.9 \pm 1.7) \times 10^{36}$	3.8 ± 0.2	0.09	(8)
FS Aur	Dwarf nova (IP)	$(1.3 \pm 0.1) \times 10^{32}$	$(2.0 \pm 0.1) \times 10^{37}$	5.7 ± 0.1	0.04	(8)
YZ Cnc	Dwarf nova	$(3.7 \pm 0.8) \times 10^{32}$	$(6.8 \pm 1.9) \times 10^{37}$	5.8 ± 1.2	0.09	(8)
V485 Cen	Dwarf nova	$(4.7 \pm 0.1) \times 10^{31}$	$(4.5 \pm 0.2) \times 10^{36}$	3.8 ± 0.5	0.11	(8)
VW Hyi	Dwarf nova	$(2.4 \pm 0.3) \times 10^{32}$	$(3.2 \pm 0.6) \times 10^{37}$	6.2 ± 0.9	0.02	(8)
X Leo	Dwarf nova	$(8.0 \pm 0.1) \times 10^{32}$	$(1.8 \pm 0.1) \times 10^{38}$	6.6 ± 0.3	0.09	(8)
BI Ori	Dwarf nova	$(3.7 \pm 0.2) \times 10^{32}$	$(8.5 \pm 0.1) \times 10^{37}$	7.0 ± 0.3	0.07	(8)
AT Cnc	Dwarf nova	$(6.9 \pm 0.3) \times 10^{32}$	$(2.1 \pm 0.3) \times 10^{38}$	7.7 ± 0.3	0.05	(8)

Note. The luminosities and energies are in TESS or Kepler bands.
References. (1) This work; (2) Scaringi et al. (2022c); (3) Scaringi et al. (2017); (4) Littlefield et al. (2022); (5) Scaringi et al. (2022b); (6) Veresvarska et al. (2024); (7) Ramsay et al. (2021); (8) Otulakowska-Hypka et al. (2016).

are more energetic than the normal flare in MQ Dra, we expanded the comparison to superflares in single main-sequence stars (Tu et al. 2020). The superflare properties have been transformed to the g filter from bolometric values using corrections from Chen et al. (2019).

In order to estimate the frequency of bursts we follow Equation (9) of Tu et al. (2020), i.e., the frequency of bursts is equal to the number of bursts divided by the continuous monitoring period. In the case of bursts that were occurring only during a low state of the system, we measured burst frequency only during the time interval when the bursts were present, rather than the entire monitoring window (i.e., during a low state of MV Lyr and TW Pic; see, e.g., Scaringi et al. 2022c).

The start of a burst was assumed to be at a time when the flux of the object visibly rose above the quiescent or noise level. The burst end was assumed to be at a time when the brightness returned to the preburst level. We note that in some of the objects, the measurements of the start and end points of a burst might have been affected by the changes in brightness due to orbital variability. Therefore, the measured duration of bursts might have a systematic error of up to a few percent.

The collected sample of bursts in CVs is presented in Table 1. The final reported values are the mean of measurements for all of the observed bursts with the reported range corresponding to the largest deviation from the mean of an individual outburst. We note that none of the measured energies or luminosities have bolometric correction. However, they are measured in a consistent fashion, i.e., they are measured in the TESS or Kepler bands and calibrated to either g or V bands.

3. Results

As a result of the comparison between the bursts, we discovered that the burst properties appear to fall into separate clusters that seem to not be connected. This suggests different physical mechanisms behind bursts in each cluster. In fact, these clusters appear to be consistent with the classification suggested in the literature, namely micronovae, magnetic gating bursts, dwarf novae, and donor flares (Figure 2). We note that Hameury et al. (2022) questioned the micronova interpretation and suggested that micronovae can be interpreted as magnetic gating bursts instead. However, it is immediately clear that systems classified as micronovae have energies orders of magnitude higher compared to bursts that were identified as magnetic gating (Table 1). This confirms that magnetic gating and micronovae are two different phenomena (Scaringi et al. 2022b). The previous confusion between micronovae and magnetic gating is likely due to the fact that the energies of the bursts were not included in the analysis of Hameury et al. (2022).

We propose that the four panels in Figure 2 can be used as diagnostic diagrams that can differentiate between the burst types. A distinction between magnetic gating bursts and stellar flares based solely on energies is not possible. Instead, one has to rely on a relationship between flares/bursts frequency and their average duration (Figure 2). In particular, there is an apparent anticorrelation between magnetic gating bursts' average duration and their frequency. The anticorrelation between the frequency of magnetic gating bursts and their duration may be expected, as lower burst frequency implies a higher mass that was halted in the accretion disk between the bursts. We note that the micronovae-measured frequency is likely significantly overestimated, since they likely remain dormant for significantly longer periods of time compared to their continuous monitoring time. The exception is CP Pup,
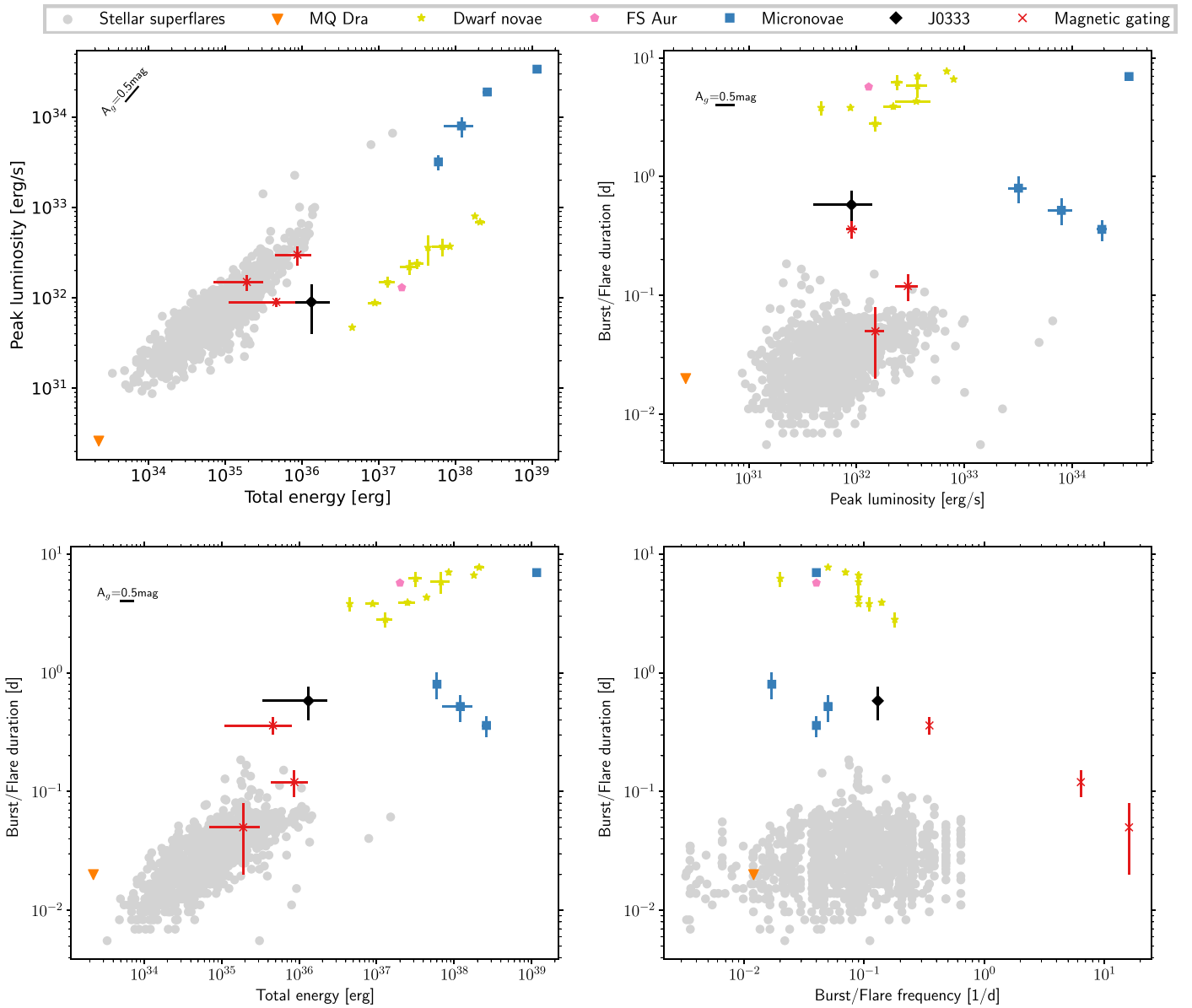
Figure 2. Properties of short bursts in CVs with their identification from the literature. Superflares from single main-sequence stars are plotted for comparison. The effect of extinction of $A_g = 0.5$ mag on the measured properties is marked with a black line.

where the recurrence time of ~ 60 days was estimated (Veresvarska et al. 2024). However, micronovae can be distinguished from other classes of bursts using other properties.

3.1. Bursts in J0333

J0333 was classified as a CV by Augusteijn et al. (2010). J0333 showed a blue continuum and emission lines of He I, He II, Fe II, and Balmer series. Based on a radial velocity study, Augusteijn et al. (2010) estimated an orbital period of the system to be 0.06 days. However, the orbital period determination was hindered by insufficient sampling of the spectroscopic observations. Moreover, the authors reported strong, short-term variations in the photometric observations of J0333. While Augusteijn et al. (2010) classified J0333 as a dwarf nova there are no recorded outbursts of the system in the literature.

J0333 experienced six bursts with varying amplitude and duration during the TESS monitoring period (Figure 1). The majority of bursts appear symmetrical, while some of the larger bursts show a fast rise and a slow decline. Moreover, the first bursts observed displayed a secondary brightening during decline.

After masking the bursts we performed a timing analysis of J0333 TESS data. A Lomb–Scargle periodogram (Lomb 1976; Scargle 1982) revealed a variability at a frequency of $14.89686(6)$ days^{-1} (97 minutes), which we identify as the orbital period (Figure 3). This orbital period is consistent with the radial velocity study done by Augusteijn et al. (2010). Moreover, we discover variability at a frequency of $37.6422(1)$ days^{-1} (38 minutes). We associate this variability with the white dwarf spin period, suggesting an intermediate polar nature of J0333. The source was detected in X-rays by Swift-X-ray Telescope (XRT) and cataloged as 2SXPS J033320.3-445139 (Evans et al. 2020). The Swift-XRT signal-to-noise ratio (S/N) was insufficient for a detailed timing analysis, although hints of a variability at the 38 minute
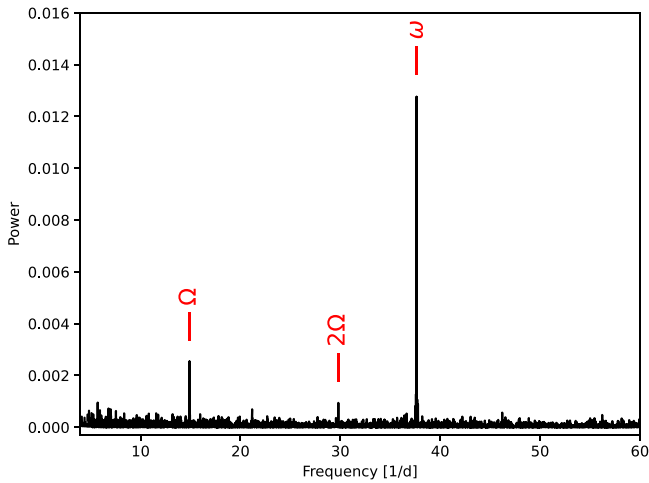
Figure 3. Lomb–Scargle periodogram of J0333 TESS observations after the bursts have been masked. Detected periodic variability corresponds to the orbital period (Ω) and the white dwarf spin period (ω).

spin period are found. In addition, the X-ray spectrum is rather hard and consistent with an optically thin plasma at a temperature of ~ 7 keV (Appendix B), further corroborating the intermediate polar identification. However, we note that the J0333 X-ray luminosity of $\sim 10^{32}$ erg s^{-1} suggests an unexpectedly high mass transfer rate for a system with a short orbital period.

The properties of J0333 bursts observed by TESS are presented in Table 1. The energies of bursts are similar to both magnetic gating bursts and stellar flares. However, the relatively long duration of bursts identifies J0333 as a magnetic gating system (Figure 2).

4. Discussion and Conclusions

We showed that short bursts in CVs display distinct observational properties that divide them into separate groups consistent with their literature classification. Based on that, we proposed diagnostic diagrams that can distinguish between the short optical burst types in CVs. The main conclusion from these diagrams regards intermediate polars. Namely, short dwarf nova outbursts in intermediate polars were speculated to be less likely to occur compared to nonmagnetic systems (Hameury & Lasota 2017). However, the properties of bursts in an intermediate polar FS Aur (Neustroev et al. 2013) are only consistent with the dwarf nova nature of the system (Figure 2). Moreover, micronovae and magnetic gating intermediate polars are separated on the diagnostic diagrams, contrary to the recent suggestion in the literature (Hameury et al. 2022). We note that this does not confirm the physical mechanism suggested for these bursts in the literature, but simply it implies a different physical mechanism is at play in micronovae and magnetic gating systems.

While all micronovae are separated from other classes of short bursts, there is a clear divide between them. Namely, the burst in ASASSN-19bh has a duration and total energy 1 order of magnitude larger compared to other micronovae. Together with the different shapes of bursts, this mimics the two types of Type-I X-ray bursts, as was noted by Scaringi et al. (2022b). However, the comparison to Type-I X-ray bursts is limited due to the fact that the nuclear reactions expected in Type-I X-ray bursts and micronovae differ. Moreover, when a larger sample of systems is discovered, it will be possible to improve the

populations in the diagnostic diagrams allowing us to confirm or disprove the segregation of different micronovae. Nevertheless, the shared relationship between the total energy released and peak flux during an outburst of the currently known sample seems to suggest that they are indeed two classes of the same phenomenon (Figure 2). If we consider the short-duration micronovae alone, it seems that there is an apparent relationship between the burst duration and peak luminosity. While only three such systems are known, the possibility of using short-duration micronovae as distance indicators should be investigated when a larger sample of objects is discovered.

Bursts in intermediate polars have been proposed to be connected to the appearance of superhumps (Mukai & Pretorius 2023). However, since we have shown that micronovae and magnetic gating bursts seem to be two separate phenomena, it seems that superhumps are only connected to the occurrence of short-duration micronovae and do not appear in magnetic gating systems.

We identified J0333 as an intermediate polar with an orbital period of 97 minutes and a white dwarf spin period of 38 minutes. Moreover, we derived diagnostic diagrams that identified short bursts discovered in J0333 as a signature of magnetic gating. J0333 has a relatively high spin-to-orbital period ratio of 0.39. The orbital period of J0333 and its spin-to-orbital period ratio is very close to what is observed in EX Hya, V598 Peg, V1025 Cen, and DW Cnc (see Figure 5 of Littlefield et al. 2023). Interestingly, EX Hya, V1025 Cen, and DW Cnc variability has been interpreted as magnetic gating bursts (Mhlahlo et al. 2007; Duffy et al. 2022; Littlefield et al. 2022). This suggests that magnetic gating in intermediate polars with a high spin-to-orbital period ratio may be common.

Appendix A
Long-term Variability of J03333

The variability of J0333 on long timescales was analyzed using data from the Catalina Real-time Transient Survey (Drake et al. 2009), All-Sky Automated Survey for Supernovae (ASAS-SN; Shappee et al. 2014; Kochanek et al. 2017), and Gaia mission (Gaia Collaboration et al. 2016; Babusiaux et al. 2023). The long-term variability of J0333 is presented in Figure 4. Similar bursts to what is observed in TESS are present during most of the monitoring period in the g band (Figure 4). The presence of the bursts before that time is inconclusive due to the lower cadence of the data, but at least one burst seemed to be observed in the V band 1 day after the Swift pointing. Both the X-ray flux and UV flux in the UVM2
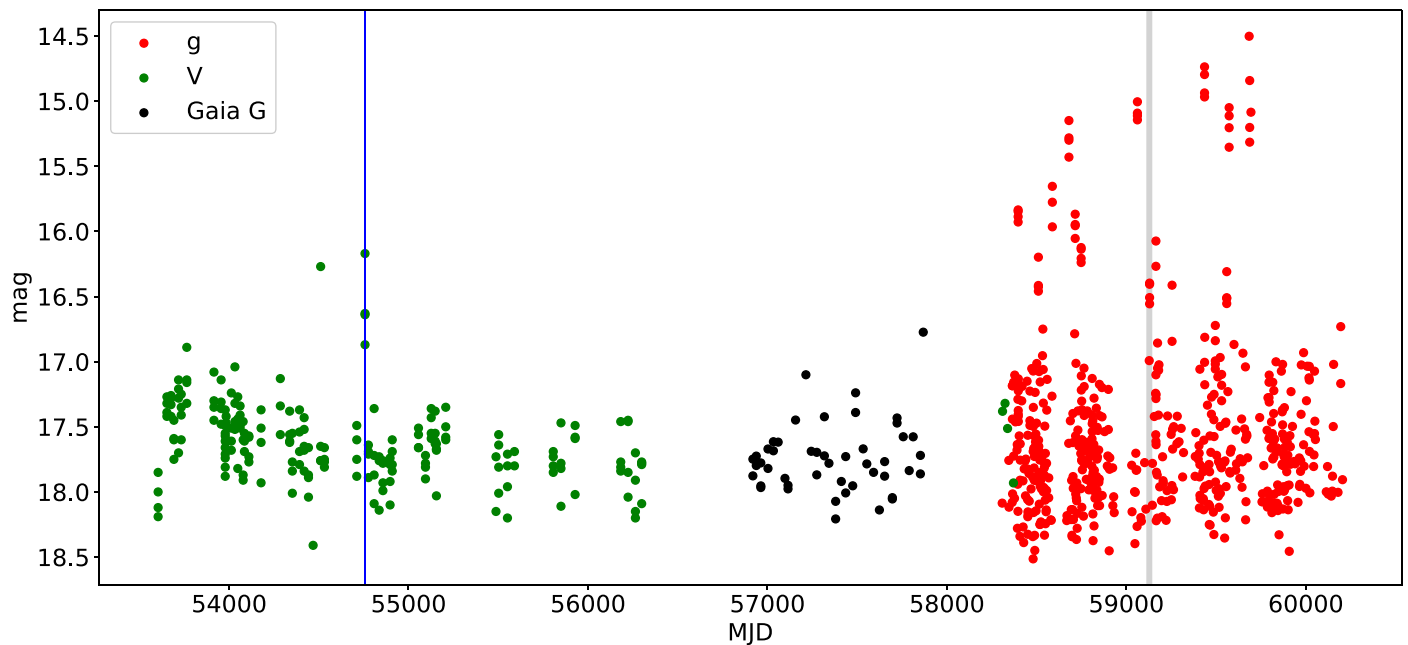
Figure 4. A light curve of J0333 in V, Gaia G, and g filters. The time of TESS monitoring is marked with a gray area. The time of the Swift pointing is marked with a blue line. The Swift pointing was 1 day after an apparent brightening in the V band.

band seemed constant during the Swift pointing, suggesting that the burst was over by the time of the Swift observation.

Appendix B
The X-Ray Emission of J0333

J0333 was observed by Swift-XRT on 2008 October 19 for $\sim$21 hr accumulating a total of 10 ks (ObsID: 00037302001). It was found at a count rate of $0.05 \, \mathrm{cts \, s^{-1}}$ in the 0.3–10 keV range. The sparse X-ray coverage due to the spacecraft orbit and the low S/N did not allow a period search but by folding the data at the 38 minute period a variability with an amplitude of $19^{+10}_{-9}\%$ was found. The X-ray spectrum averaged over the whole observation is equally fitted (C-statistic) with an absorbed power law with index $1.84^{+0.23}_{-0.22}$ ($\chi^2_{\mathrm{red}} = 1.14$) and an optically thin plasma APEC with temperature of $6.6^{+5.5}_{-1.9}$ keV adopting solar abundances ($\chi^2_{\mathrm{red}} = 1.2$) models. The more physical APEC model fit gives a hydrogen column density of $N_{\mathrm{H}} = 3.8^{+4.4}_{-0.2} \times 10^{20} \, cm^{-2}$ consistent with the small distance of J0333 and the total column density toward the source (HI4PI Collaboration et al. 2016), while the power-law fit gives a much higher value $N_{\mathrm{H}} = 1.2 \times 10^{21} \, cm^{-2}$. The unabsorbed X-ray flux for the APEC fit was $F_{0.3-10} = 1.9 \times 10^{-12} \, erg \, cm^{-2} \, s^{-1}$ and the bolometric flux over a dummy range of 0.1–100 keV resulted in $\sim$2.2 $\times 10^{-12} \, \mathrm{erg \, cm^{-2} \, s^{-1}}$. At the Gaia DR3 distance of 578 pc, the X-ray luminosity was found to be $\sim$8.8 $\times 10^{31} \, \mathrm{erg \, s^{-1}}$. The lack of better-quality data and higher energy coverage prevents us from inferring a possible temperature gradient and hence a possible estimate of the white dwarf mass.

ORCID iDs

Krystian Iłkiewicz https://orcid.org/0000-0002-4005-5095
Simone Scaringi https://orcid.org/0000-0001-5387-7189
Martina Veresvarska https://orcid.org/0000-0002-0146-3096
Domitilla De Martino https://orcid.org/0000-0002-5069-4202
Colin Littlefield https://orcid.org/0000-0001-7746-5795
Christian Knigge https://orcid.org/0000-0002-1116-2553
John A. Paice https://orcid.org/0000-0003-1149-1741
Anwesha Sahu https://orcid.org/0009-0007-6825-3230

References

Augusteijn, T., Tappert, C., Dall, T., & Maza, J. 2010, MNRAS, 405, 621
Babusiaux, C., Fabricius, C., Khanna, S., et al. 2023, A&A, 674, A32
Bailer-Jones, C. A. L., Rybizki, J., Fouesneau, M., Demleitner, M., & Andrae, R. 2021, AJ, 161, 147
Cannizzo, J. K., Smale, A. P., Wood, M. A., Still, M. D., & Howell, S. B. 2012, ApJ, 747, 117
Chen, Y., Girardi, L., Fu, X., et al. 2019, A&A, 632, A105
D'Angelo, C. R., & Spruit, H. C. 2010, MNRAS, 406, 1208
D'Angelo, C. R., & Spruit, H. C. 2012, MNRAS, 420, 416
Drake, A. J., Djorgovski, S. G., Mahabal, A., et al. 2009, ApJ, 696, 870
Duffy, C., Ramsay, G., Steeghs, D., et al. 2022, MNRAS, 510, 1002
Evans, P. A., Page, K. L., Osborne, J. P., et al. 2020, ApJS, 247, 54
Gaia Collaboration, Prusti, T., de Bruijne, J. H. J., et al. 2016, A&A, 595, A1
Green, G. M., Schlafly, E., Zucker, C., Speagle, J. S., & Finkbeiner, D. 2019, ApJ, 887, 93
Hameury, J. M., & Lasota, J. P. 2017, A&A, 602, A102
Hameury, J. M., Lasota, J. P., & Shaw, A. W. 2022, A&A, 664, A7
HI4PI Collaboration, Ben Bekhti, N., Flöer, L., et al. 2016, A&A, 594, A116
Iłkiewicz, K., Mikołajewska, J., & Stoyanov, K. A. 2023, ApJL, 953, L7
Jenkins, J. M., Twicken, J. D., McCauliff, S., et al. 2016, Proc. SPIE, 9913, 99133E
Kochanek, C. S., Shappee, B. J., Stanek, K. Z., et al. 2017, PASP, 129, 104502
Lasota, J.-P. 2001, NewAR, 45, 449
Littlefield, C., Lasota, J.-P., Hameury, J.-M., et al. 2022, ApJL, 924, L8
Littlefield, C., Mason, P. A., Garnavich, P., et al. 2023, ApJL, 943, L24
Lomb, N. R. 1976, Ap&SS, 39, 447
Masci, F. J., Laher, R. R., Rusholme, B., et al. 2019, PASP, 131, 018003
Mhlahlo, N., Buckley, D. A. H., Dhillon, V. S., et al. 2007, MNRAS, 380, 353
Mukai, K., & Pretorius, M. L. 2023, MNRAS, 523, 3192
Neustroev, V. V., Tovmassian, G. H., Zharikov, S. V., & Sjoberg, G. 2013, MNRAS, 432, 2596
Otulakowska-Hypka, M., Olech, A., & Patterson, J. 2016, MNRAS, 460, 2526
Ramsay, G., Doyle, J. G., & Doyle, L. 2020, MNRAS, 497, 2320
Ramsay, G., Hakala, P., & Wood, M. A. 2021, MNRAS, 504, 4072
Ricker, G. R., Winn, J. N., Vanderspek, R., et al. 2015, JATIS, 1, 014003

Scargle, J. D. 1982, ApJ, 263, 835
Scaringi, S., de Martino, D., Buckley, D. A. H., et al. 2022c, NatAs, 6, 98
Scaringi, S., Groot, P. J., Knigge, C., et al. 2022a, MNRAS, 514, L11
Scaringi, S., Groot, P. J., Knigge, C., et al. 2022b, Natur, 604, 447
Scaringi, S., Maccarone, T. J., D'Angelo, C., Knigge, C., & Groot, P. J. 2017, Natur, 552, 210
Schaefer, B. E., Pagnotta, A., & Zoppelt, S. 2022, MNRAS, 512, 1924

Shappee, B. J., Prieto, J. L., Grupe, D., et al. 2014, ApJ, 788, 48
Sokolovsky, K. V., Johnson, T. J., Buson, S., et al. 2023, MNRAS, 521, 5453
Tu, Z.-L., Yang, M., Wang, H. F., & Wang, F. Y. 2021, ApJS, 253, 35
Tu, Z.-L., Yang, M., Zhang, Z. J., & Wang, F. Y. 2020, ApJ, 890, 46
Veresvarska, M., Scaringi, S., Hagen, S., et al. 2024, MNRAS, submitted
Warner, B. 2003, Cataclysmic Variable Stars (Cambridge: Cambridge Univ. Press)